Microfluidics and Nanofluidics (2023) 27:37
https://doi.org/10.1007/s10404-023-02645-4

CORRESPONDENCE

Automated microparticle positioning using a pair of ultrasound-actuated microbubbles for microfluidic applications

Amirabas Bakhtiari[1] · **Christian J. Kähler**[1]

Received: 6 November 2022 / Accepted: 21 April 2023

Abstract
We present an advanced single-particle positioning technique that uses ultrasound-driven microstreaming induced by two microbubbles to position microparticles across the width of a microchannel or to direct them to desired exits of a Y-shaped microchannel. An open-loop control algorithm has been devised to facilitate the automatic detection, tracking, and precise positioning of microparticles in the presence of two microbubbles. Our control system is capable of performing particle positioning in multiple steps, individually for each microparticle, with arbitrary starting positions without requiring prior particle focusing or flow conditioning. We have also evaluated the accuracy enhancement of particle positioning using two microbubbles, in comparison to the system's results using only one microbubble.

Keywords Microfluidics · Microbubble · Single-particle analysis · Particle positioning

1 Introduction

Non-contact sorting of microparticles and biological cells is of great benefit for many fundamental biomedical and biological applications. Over the past decade, a variety of functions such as detection, focusing, mixing, counting, lysis, and analysis of single cells have been successfully performed using advanced lab-on-a-chip devices (Nilsson et al. 2009; Nan et al. 2014; Sheng et al. 2014; Mernier et al. 2010; Yang et al. 2006; Zhao et al. 2013). Circulating fetal cells (CFCs), enrichment of circulating tumor cells (CTCs), and hematopoietic stem cells (HSCs) (Armstrong et al. 2011; Wognum et al. 2003; Bischoff et al. 2003; Chen et al. 2014), as well as single-cell electroporation (Khine et al. 2005) and single-cell impedance spectroscopy (Han and Frazier 2006; Cho and Thielecke 2007; Chen et al. 2011; Malleo et al. 2010), are just a few examples of cell isolation that illustrate the importance of cell detection, sorting, and removal. In active cell sorting applications, external fields such as acoustic, electric, magnetic, and optical fields are typically utilized (Shields et al. 2015). However, in some cases, such as the use of a high-power laser in optical tweezers or a high electric field in electrokinetic tweezers, the cell membrane can be seriously damaged or the natural experimental environment altered. This highlights the importance of using a non-invasive and non-destructive force field for non-contact manipulation at the cellular scale.

As a non-invasive and biocompatible method for positioning cells, acoustically actuated microbubbles in microchannels can be used, where the vibration of the bubbles can generate micro streaming in the form of counter-rotating vortices (Riley 2001; Marmottant and Hilgenfeldt 2003; Versluis et al. 2010). The microstreaming can be controlled by manipulating the frequency and amplitude of the applied driving force, thus allowing for flexibility in accommodating various microchannel configurations, including minor changes in flow rates and channel geometry (Ahmed et al. 2016; Rallabandi et al. 2014; Wang et al. 2013). This level of control would be challenging to achieve with a binary on-off approach that relies on unregulated force fields that can only divert particles away from the main flow towards an outlet (Chen et al. 2014). Through the utilization of microbubble streaming, micro-particles and biological cells exhibiting varying physical properties, such as size, shape, density, and compressibility, can be accurately transported to specific lateral positions within microchannels. This method holds universal applicability in all microfluidic areas, provided that

✉ Amirabas Bakhtiari
amirabas.bakhtiari@unibw.de

[1] Institute for Fluid Mechanics and Aerodynamics, Fakultät für Luft- und Raumfahrttechnik, Universität der Bundeswehr, Werner-Heisenberg-Weg 39, 85579 Neubiberg, Bayern, Germany

Published online: 09 May 2023

the density of the particles is negligibly different from that of the main fluid. However, if the Stokes number greatly exceeds unity, the positioning process may necessitate a longer period and, in certain circumstances, may fail to yield desired results. Since the concept is based on oscillating microbubbles and no moving parts are involved, the positioning device is robust for long-term operation as there is no particular need to maintain or clean the integrated parts on the microchip.

In a recent study, an automated system that uses one actuated microbubble was developed and qualified to precisely move single microparticles across the width of a microchannel to desired locations for their rejections for instance (Bakhtiari and Kähler 2022). It has been shown that in the presence of Poiseuille flow, the effective range of a microbubble streaming in which the flow can effectively manipulate the particles is limited by the critical value of the transducer amplitude and the relatively fast Poiseuille flow. This limits the single bubble technique to small channel dimensions.

Multi-step positioning using two microbubbles in opposing walls could be an alternative approach to improve results in wider microchannels or at higher flow rates. To explain this idea, we investigate in this study the effects of two microbubbles on the accuracy of single-particle positioning and explained in detail the combined Poiseuille flow with these two microflows arranged orthogonally in the microchannel. To this end, we developed a new control system compatible with the operation of the system in the presence of two microbubbles. We have additionally devised an active methodology to rapidly regulate the dimensions of air bubbles within the microchannel, with the aim of ensuring sustained and reproducible outcomes over prolonged periods of time. This method can be accomplished within a few seconds (usually 0.5~1 s) and is considered essential for the efficacy and dependability of the overall process.

2 Experimental setup

This section explains the solution preparation and the experimental setup, which consists of three main parts: a microfluidic system, an optical setup, and the control system, which are mounted on a vibration-damped table to minimize experimental errors.

2.1 Solution preparation

In this experimental study, polystyrene microspheres with a diameter of 2 μm were utilized. These microspheres were procured from Microparticles GmbH and were suspended in an aqueous solution containing 23.8 w-w% glycerol. The suspension was vigorously mixed to ensure uniform distribution of the microspheres throughout the solution. This was done to guarantee that the particles entered the channel at a random y-position and at a nearly constant rate of particles per unit of time. The aim of using this solution was to achieve particles with neutral buoyancy by ensuring that their density was equivalent to that of the surrounding medium. To determine the behavior of the particles in the fluid, we calculated the Stokes number, which was found to be $\mathrm{Stk} = 3.9\times10^{-5} << 1$ based on the experimental parameters. As a result, the particles followed the streamlines of the fluid closely.

2.2 Microfluidic chip

A schematic of the microfluidic experimental setups consisting of microchannels and flow control systems is shown in figure 1. When a microbubble is subjected to piezo-transducer excitation within a microchannel, the resulting surface oscillations of the bubble are transferred to the surrounding fluid, thereby generating a primary oscillatory flow. This primary flow, in the presence of the microchannel walls, induces a secondary flow pattern characterized by counter-rotating vortices (Marin et al. 2015; Riley 2001; Marmottant and Hilgenfeldt 2003; Versluis et al. 2010). The microchannel with height H=100 μm, width W=500 μm and length L=20 mm has the side pits with width w=80 μm and length h=200 μm spaced 1500 μm apart. Following previous studies (Wang et al. 2013; Rallabandi et al. 2014; Ahmed et al. 2016; Tovar and Lee 2009; Ahmed et al. 2009), the width of the pits was chosen to be not too wide to avoid significant 3D flow phenomena around the bubble and not too narrow to create a very small bubble with minimal impact on the flow field. The microchannels were fabricated using

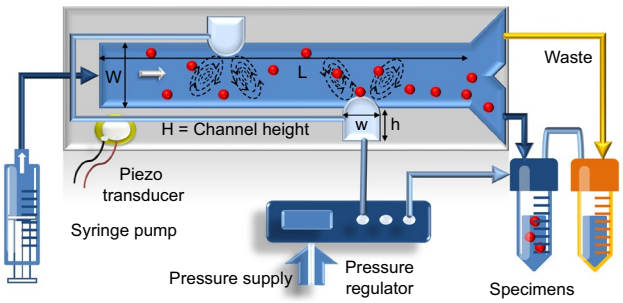

Fig. 1 Schematic of the microfluidic chip and the flow control system. The PDMS microchannel of width W, height H, and length L has two side cavities of width w and length h spaced apart (1500 μm in this work). The cavities in (PDMS) are interconnected through a side channel that is further linked to the pressure regulator through the tubing. The microbubbles are excited by a piezoelectric transducer and generate primary oscillatory flows that lead to secondary flows in the form of counter-rotating vortices. The flow rate is controlled by the syringe pump, and the pressure regulator adjusts the pressure of the liquid and bubbles to stabilize their size

the standard soft lithography method, analogous to the approach described by Wang et al. (2012). The flow rate within the microchannel is regulated using a syringe pump (neMESYS), which allows for precise control over the volume of sample solution introduced into the system. To maintain a constant bubble size, a pressure regulator (Fluigent-MFCS^T*M*-EZ, 0–1000 mbar, France) is employed to adjust the pressure differences between the outlet and interior of the bubbles.

2.3 Optical setup

The microfluidic chip is placed on the three-dimensional motorized stage of an upright Zeiss AxioImager.Z2 microscope equipped with a dichroic filter and a 10× objective (EC Plan Neouar 10×/0.3 M27) to which an sCMOS camera (pco.edge 5.5) is mounted. The proposed system is capable of being operated in both bright-field and dark-field modes with a signal-to-noise ratio (SNR) suitable for detecting different types of particles. In bright-field microscopy, the particles are illuminated from behind, and the camera captures the shadow of the particles. In epifluorescence microscopy, fluorescent particles are illuminated by a continuous-wave laser or a high-power LED through the optical path, and the camera records the fluorescent light emitted from the particles. As fluorescent particles were used in this study, epifluorescence microscopy was preferred over bright-field microscopy due to its higher SNR. This makes it possible to detect particles without capturing unwanted features such as impurities or channel contamination during imaging. The detection of particles can be achieved by simple thresholding during processing, which significantly reduces the processing time and error rates as compared to bright-field microscopy. In bright-field microscopy, a longer processing process is required, such as inverting the raw images, removing the background, and correcting the particle shape.

2.4 Control system setup

Lab-VIEW (National Instrument, USA) is used to perform and simultaneously control the entire process of image acquisition, image analysis, and particle positioning in live mode through a custom-designed feedback system. The feedback control system consists of a function generator (GW INSTEK AFG-2225), an amplifier (Krohn Hite 7500), and an oscilloscope (Teledyne LeCroy HDO6104) to transmit the predefined electrical signal to a piezoelectric transducer mounted on the microfluidic chip. The function generator is triggered by a National Instruments USB-6002 DAQmx data acquisition device that receives commands from Lab-VIEW (see Fig. 2).

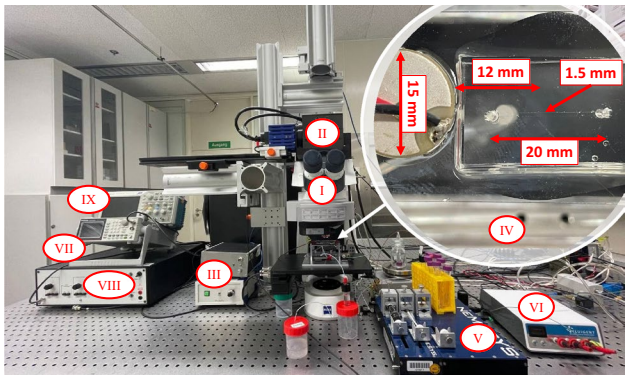

Fig. 2 The experimental setup consists of a microfluidic system, an optical setup, and a control system. The optical setup consists of an upright microscope with a 10× objective (I), a camera (II), and light sources (III). The microfluidic setup consists of the microfluidic chip and the piezoelectric transducer. The piezoelectric transducer is positioned at a distance of 12 mm from the first cavity (A) and 13.5 mm from the second cavity (B) within a microchannel that is 20 mm in length (IV), a syringe pump (V) that charges the flow into the channel, and a pressure controller (VI) to control the bubble size. Finally, the piezoelectric element is activated by a function generator (VII), an amplifier (VIII), and an oscilloscope (IX) controlled by LabVIEW

2.5 Methods

The principle of particle positioning with two microbubbles in this study follows a similar basis as the approach described in Bakhtiari and Kähler (2022) for the system with one microbubble. In this context, the initial position of each incoming particle is detected, given that all particles possess random y-positions. If it does not match the intended final y-position (y_t) at the end of the channel, the microbubble is activated to initiate the streaming with the aim to pull the particle up or down until it reaches the desired location y_t (see Fig. 3). At this moment, the piezo element is deactivated so that the particle remains at the same spanwise location (y-direction) as y_t for the rest of its path. The FOV, or field of view, is set to image the entire area in which particle positioning takes place. Typically, this area is the effective microstreaming region, as illustrated in figure 4. During operation, the FOV may be displayed to the operator for monitoring purposes or turned off when not in use. Since it is unnecessary to manipulate particles outside of the ROIs (regions of interest), only data from within the ROIs of the raw images are selected for particle positioning processing. This approach enables faster operation in live mode. The data from the ROIs are processed simultaneously and the results can be visualized to the operator individually or together, either before or after processing, such as with raw or binary images. If desired, the visualization of the results can be turned off (for more details see Bakhtiari and Kähler (2022)). However, the use of two microbubbles requires a more comprehensive, complex, and faster control system and

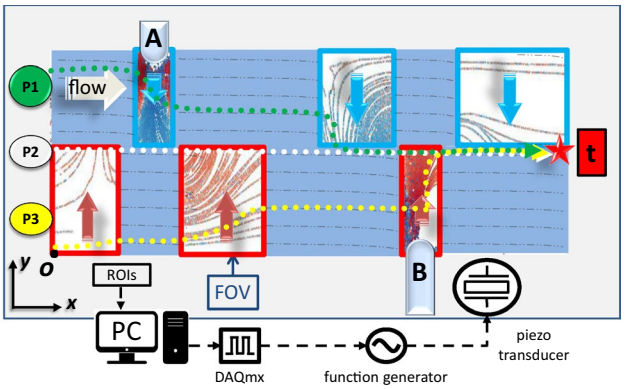

Fig. 3 The principle of positioning single particles with the help of two microbubbles ($y_{p\text{-green}} > y_t, y_{p\text{-white}} = y_t, y_{p\text{-yellow}} < y_t$). Upon the entry of a particle into the regions of interest (ROIs), the piezoelectric transducer is activated, resulting in the excitation of microbubbles and the generation of microstreaming. This phenomenon induces downward flows and upward flows in the blue and red ROIs, respectively. The excitation persists until the particle is removed from the ROIs and positioned at the same spanwise location (y-direction) as y_t

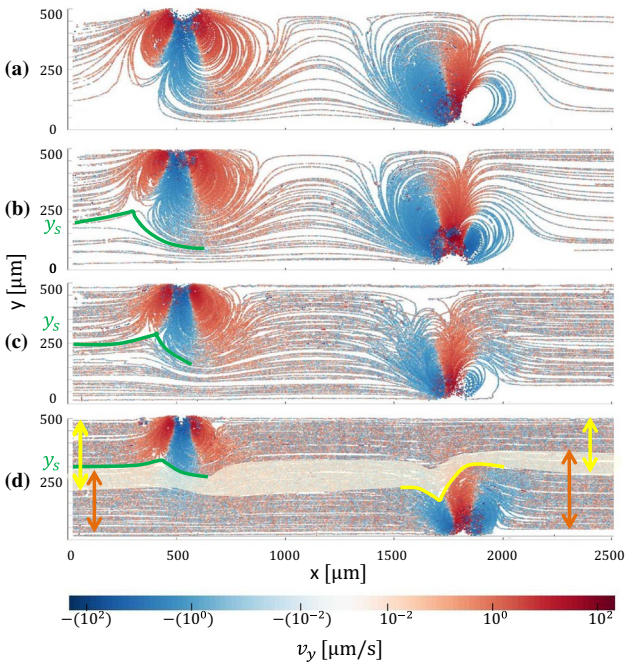

Fig. 4 The results of tracking 2 μm particles in a combined Poiseuille flow (from left to right) with the microbubble streaming when the bubbles are continuously oscillated by an excited piezoelectric transducer with 75 V_{pp} at (18.9 kHz). The y_s value indicates the y-position of the separatrix streamline at x=0. The region highlighted in d denotes an area where particles (located between the first and second separatrix) pass through both bubbles streaming without significant alterations in their y-positions

a more advanced microfluidic system to hold and stabilize two bubbles than the single microbubble system.

2.5.1 Advanced control system

We have designed and implemented an open-loop control mechanism that utilizes ultrasound-induced microstreaming of a pair of microbubbles to direct microparticles toward predetermined outputs of a Y-shaped microchannel or position them across the entire width of a straight microchannel in live mode. Control algorithms with different functionalities are integrated into the system to detect the intended single particle, activate the piezoelectric transducer to initiate the microstreaming, and track the particle to reach the target position, whether the target is defined manually by the operator or automatically by moving the mouse pointer in live mode. The control system has been considerably enhanced to cover a wider field of view (FOV) and to use more regions of interest (ROIs) that can be placed in more regions of upward or downward flow, giving the system more opportunities to adjust the position of the particles, resulting in significantly higher positioning accuracy compared to Bakhtiari and Kähler (2022), which could only work with one microbubble. In this way, particle positioning is performed in multi-steps exclusively for each microparticle with an arbitrary starting position that does not rely on prior particle focusing or any kind of flow conditioning before the operation. However, as will be discussed in more detail in the next sections, it should be noted that the technique is designed for the high-resolution positioning of only one particle in the FOV at a time. Moreover, for a given flow velocity, the best results are obtained when the superposition of Poiseuille flow and microbubble streaming (Summation of the spans of the vortices of the bubbles) can completely cover the entire width of the microchannel.

2.5.2 Active size control of two microbubbles

When a fast flow is introduced into a microchannel, quasi-cylindrical microbubbles become trapped within the lateral pits. To ensure a relatively similar pattern of microbubble streaming, a similar protrusion depth (d) of two microbubbles should be achieved. In general, the bubbles grow and shrink unevenly due to gas transport through the porous PDMS channel walls, which can be passively corrected by connecting the lateral pits to force pressure equalization (see in Volk (2020)). However, this can take a very long time, and in some cases, it may never be compensated for due to the long, narrow, and uneven channel connection. To achieve rapid and stable leveling of the bubble surfaces, the cavities can be connected together or individually to the pressure regulator so that the size and shape of the bubble can be quickly (usually 0.5~1 s) adjusted by changing

the gas pressure inside the microbubbles. As illustrated in Fig. 1, the flow rate within the microchannel was accurately regulated using a syringe pump, while the pressure differential between the microbubbles' interior and outlets was simultaneously controlled through a pressure regulator. In our experimental setup, the cavities are interconnected by a side channel, and a pressure difference of approximately 6–8 mbar is maintained within the microchannels.

3 Results and discussion

In this section, a set of practical experiments was carried out in two Y-shaped microchannels, each of which accommodated one or two microbubbles. Moreover, statistical experiments were conducted in a straight microchannel made of polydimethylsiloxane (PDMS), which accommodated two microbubbles, to analyze the combined Poiseuille flow with microbubble streaming. Finally, the uncertainty of single-particle positioning was evaluated in the same microchannel and compared to the findings of the previous study, which featured a microchannel containing one microbubble.

In previous work, in the presence of Poiseuille flow, the effective range of single-microbubble streaming in which flow can effectively manipulate particles was characterized. It was found that the lateral flow was limited by the critical value of the transducer amplitude and the relatively fast Poiseuille flow, so particles beyond this range (near the opposite wall of the bubble) could not be precisely directed. Positioning particles in multiple steps using a pair of microbubbles in opposing walls can improve results in wider microchannels or at faster flow rates. In this work, the effect of using two microbubbles on the positioning of a single microparticle in a microchannel is investigated.

3.1 Effective streaming domain

To achieve efficient particle displacement through the shortest path, it is advantageous to utilize vortices that are minimally complex. Volk and Kähler (2018) demonstrated that the most rapid microstreaming can be attained when the protrusion depth of the bubble is equal to one-quarter of the cavity width (i.e., $d = w/4$, where w represents the width of the cavity). In this investigation, we achieved the same protrusion depth by regulating the pressure differential between the bubble interior and the outlet. We then systematically increased the excitation frequency until the point at which the strongest vortices were observed. The General Defocusing Particle Tracking (GDPT) technique was used to track the trajectory of 2 μm tracer particles in a glycerol-water solution with high particle concentrations when the particles were exposed to a complex flow field resulting from the superposition of a Poiseuille flow (from left to right) and the microstreaming generated by two microbubbles with a diameter of $d = w/4$. The flow field was characterized at different Poiseuille flow velocities, while microbubbles were excited at f_r=18.9 kHz with $V_r = 75\ V_{pp}$.

The findings are depicted in figure 4a ($V_m = 268, \mu m/s$) demonstrate that the streaming of both bubbles can successfully draw all the particles, even those farthest from the bubbles, into the core of the vortices. This means that each of the bubbles is individually capable of positioning the target particles across the entire width of the microchannel. The dissimilar pattern observed in the second pair of vortices can be attributed to variations in inflow conditions. Specifically, the first bubble streaming experiences a pure Poiseuille flow, whereas the second pair of vortices is subject to a modified inflow incorporating both the Poiseuille flow and the first set of counter-rotating vortices. Increasing the mean flow velocity (Fig. 4b) results in the formation of an asymptotic point at the bottom of the upstream vortex, which can be identified by a corresponding critical streamline or separatrix (also see Bakhtiari and Kähler (2022); Thameem et al. (2016)). Particles located below this separatrix ($y_p < y_s$, in this case, y_p <230 μm, where y_p is the y-position of the particle and y_s is the y-position of the separatrix) avoid proximity to the bubble and avoid being affected by the upward flow of the vortices. As a result, the first bubble is unable to manipulate all of the incoming particles (those located below the separatrix-green line) individually. In the following, the particles that escaped the vortices move directly to the second pair of vortices with small changes in their lateral position, while the particles above the separatrix line are pulled into the vortices and, after some rotations in the loops near the first bubble surface, leave the vortices with positive lateral velocity components and are captured by the vortices of the second bubble. The second pair of vortices span the entire width of the microchannel and can potentially position any particles leaving the first vortices at any lateral height. When the mainstream is further increased to 622 μm/s (Fig. 4c), the range of incoming particles that can be manipulated by the first bubble is further limited and the separatrix moves closer to the bubble ($y_s = 275\ \mu m$). In this case, except for two particles with maximum y_p, the rest of the particles passing from the first bubble can be dragged to the second pair of vortices which are expanded across the width of the channel. The positioning of these two critical particles can be done in two steps so that the first streaming can bring them to a lower lateral level (e.g. y_p <450 μm), where the second vortices can easily gather them and drive them to the target position (y_t). However, figure 4c displays the maximum main flow velocity (622 μm) in this configuration, with which the system is able to position particles with any initial lateral values, while the maximum flow rate for a single bubble configuration was observed at 536 μm/s, that even precise positioning was not possible for

particles far from the microbubble (see Bakhtiari and Kähler (2022)). A further increase of the flow rate to 1400 μm/s results in a slight increment of the lateral height of the separatrix to $y_s = 285\,\mu m$. This change, although small compared to Fig. 4(c), has a significant impact on the effective manipulation area of the second bubble. This reduction in the manipulation area allows particles with a lateral value greater than 220 μm to escape the second bubble streaming without controllable manipulations. Consequently, particles with $y_p > y_{s_2}$ cannot reach the lower part of the channel (orange area), and particles with $y_p < y_{s_1}$ cannot be positioned in the upper part downstream of the microchannel (yellow area), rendering the system incapable of exploiting two microbubbles.

3.2 Single-particle positioning via two microbubbles

3.2.1 Y-shaped microchannel

In many applications, it is often of interest to remove or separate rare cells or other impurities from the fluid through one or more side channels. In this study, we put the technique into practice and demonstrate the integration of single-particle positioning in a practical application of a Y-shaped microchannel to direct all (even for selected particles) into a specific outlet. To achieve this, a side pit is located upstream of the intersection of the Y-shaped microchannel to accommodate a microbubble. Changing the shape and geometry of the microchannel will significantly affect the pattern and intensity of microbubble streaming. Therefore, the bubble and the junction are far enough apart (100 μm in this study) to avoid any disturbance of the general pattern of counter-rotating vortices when the bubble is excited by piezoelectrics. The first set of experiments was performed in a 500- μm microchannel with one microbubble. The Poiseuille flow rate of 220 $\mu m/s$ was driven into the channel and evenly distributed to the side channels at the end of the microchannel.

Figure 5 shows the results when the 2 μm particles are directed into the upper (250–500 μm) or lower (0–250 μm) side-channel (outlet). To deliver the particles into the upper channel (collect), all particles must be positioned in the range of 250–500 μm before they reach the intersection. As shown in the previous study, the fast upward flow directly above the activated microbubble can bring the microparticles close to the opposite side of the microbubble. Therefore, an ROI is placed above the microbubble extending from the bubble surface to a height higher than half of the channel (410 μm in this study) so that all the incoming particles with a lateral position $y_p < 250\,\mu m$ enter this ROI and can be detected. At this moment, the piezoelectric transducer is activated until the generated upward flow evicts the particles from the ROI to the upper half of the channel, where they can be transported by the incoming laminar flow to the collect outlet through the upper side channel. In case (b), the goal is to position all particles in the lower half of the microchannel. To do this, we use the downward flow that exists upstream and downstream of the activated microbubble. When the particles with $y_p > 250\,\mu m$ enter the ROIs, the piezoelectric transducer is activated, resulting in a downward flow in these regions that pulls the microparticles to a lower lateral level. Similar to the first case, the piezoelectric transducer is deactivated when the particles leave the ROIs, and they follow the laminar flow and eventually exit via the lower lateral channel.

For case (a), the upward flow is only required to lift particles above the microchannel center, not its entire width. Thus, higher Poiseuille flow rates can be used if the microbubble streaming height is greater than half the

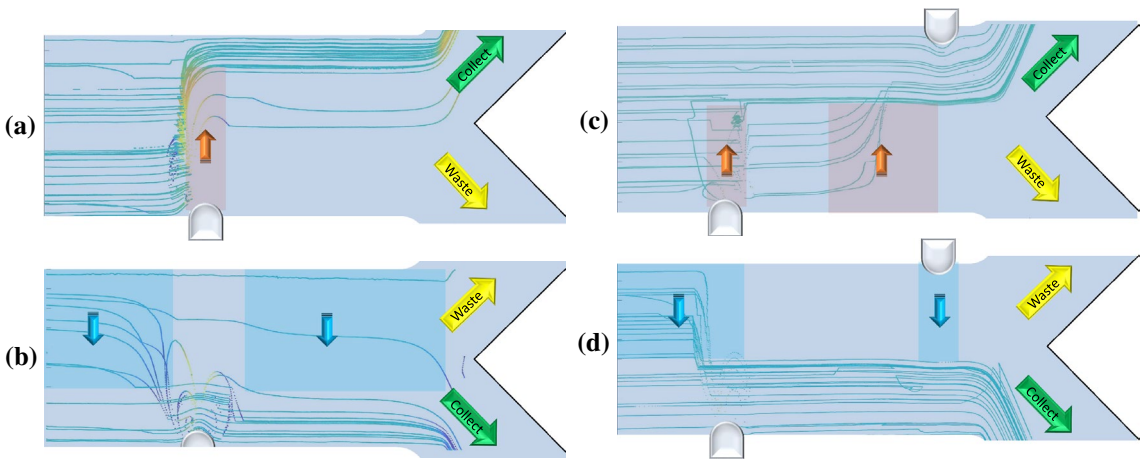

Fig. 5 Particle tracking of 2 μm particles directed into the collection outlet with one microbubble (**a** and **b**) and two microbubbles (**c** and **d**)

microchannel height. In contrast, the second case requires strong microstreaming to pull particles at the farthest distance from the microbubble. This can be difficult in wider channels, higher flow velocities, or when particles are close to the opposite wall. In Fig. 5b, at least one microparticle was unable to enter the lower half of the microchannel before exiting through the upper side channel at the intersection. To overcome this problem and enhance the efficiency of the technique, a second pit is introduced on the opposite wall of the first bubble to accommodate the second bubble. The results of this modification are demonstrated in Figure 5(c, d), which reveal that the inclusion of the second bubble substantially enhances the outcome, as all particles can be successfully directed towards the selected outlet in both cases. Here, the system takes advantage of both streaming futures of counter-rotating vortices, the relatively wider dragging streaming upstream and downstream of one bubble and the relatively stronger pushing streaming directly at the surface of another bubble, in a unified direction. This approach facilitates the positioning of particles via a multi-stage process. Specifically, particles in close proximity to the $y = 0$ plane, which cannot achieve the desired vertical positioning through the initial bubble streaming process, undergo a secondary attempt downstream utilizing a second microbubble positioned on the opposite side of the channel. This additional step could potentially advance their trajectory toward the intended outlet. Through this mechanism, the system can achieve enhanced performance at increased flow rates, and can even operate within wider microchannels due to the capacity of microbubble streaming to encompass a greater lateral area.

3.2.2 Quantifying the positional uncertainty of particles in a straight microchannel

A series of experiments were performed to determine the uncertainty in the positioning of single particles (with random y-positions) via two microbubbles. The objective was to position individual particles in 5 different areas of 10 μm along the width (y direction) of the microchannel with a width of 500 μm and a height of 100 μm. In this microchannel, the lateral pits are spaced 1500 μm apart and the microbubbles ($w = 80\ \mu m$, $d = w/4$) oscillating at $f_r = 18.9$ kHz and $V_r = 70\ v_{pp}$ when microparticles are in the ROIs. For accurate positioning of individual particles within the field of view, only one particle should be present at any given time. To achieve this, a low concentration of 2 μm particles in the glycerol-water solution (23.8% w/w) was utilized. Data pertaining to time points with the presence of more than one particle were excluded from the calculation to ensure data accuracy. The particle suspension is introduced into the microchannel via a syringe pump operating at a flow rate of 0.014 $\mu l/s$, and the height of the bubble surface is kept constant by controlling the outlet pressure with the Fluigent pressure regulator between 7–8 mbar above atmospheric pressure. For each case, an average of 28 valid particles were captured during 20 min of live operation (100 frames per second).

Fig. 6 displays a comparative analysis of the median value and median absolute deviation, as represented by error bars, for five distinct positioning cases involving 2 μm particles. The particles were positioned using either one microbubble (indicated by red error bars from figure 10 in Bakhtiari and Kähler (2022)) or two microbubbles (indicated by blue error bars) within the predetermined target range. In the depicted figure, green rectangles demarcate the target range for each of the five scenarios. The system aims to achieve particle positioning within a ten-micron range, and the process terminates upon the attainment of this 10-μm threshold. For the case one of the experiments with two bubbles (blue error bars), the control system aims to focus the particles in a range of $45< y_t <55\ \mu m$ near the bottom wall, so there is no need to move the particles to a higher lateral position. Therefore, the ROIs are placed downstream and upstream of the lower bubble (y_{b_1}=0) and directly below the surface of the upper bubble ($y_{b_2} = 500\ \mu m$) in the areas where there is only downward streaming resulting in positioning with a median value of $y_{p_f} = 52.8\ \mu m$ and median absolute deviation of $MAD_f = 3.8\ \mu m$. In the next steps, in cases two to four, the particles should be focused by downward and upward flows of the two bubbles in the range of $145< y_t <155\ \mu m$, $245< y_t <255\ \mu m$, and $345< y_t <355\ \mu m$, respectively. For this purpose, ROIs are appropriately placed in the upward flow and downward flow regions and spanned from the walls to the target positions (y_t), resulting in single-particle positions of $\tilde{y}_{p_f}$ of 160.05, 256.9 and 350.5 μm with MAD_f of 5.2, 7.15, and 6.5μm for C2, C3, and C4, respectively. In Case 5, the particles should be positioned near the upper wall in the region of $445< y_t <455\ \mu m$, so the ROIs are placed only in

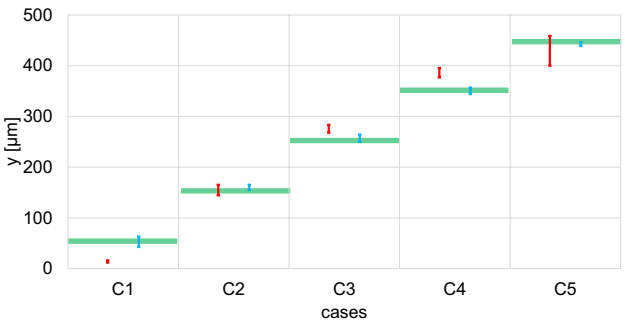

Fig. 6 The median value and median absolute deviation of the 5 cases of positioning 2 μm particles with one microbubble (red error bars) and two microbubbles (blue error bars) within the target range (green rectangles show the target range for each case)

the regions of upward flow (downstream and upstream of the upper bubble and above the bottom bubble, where the fast upward flow is present), resulting in positioning with a median value of $\tilde{y}_{p_f} = 442.8\ \mu m$ and a median absolute deviation of $MAD_f = 3.9\ \mu m$.

A comparison of the results of similar cases with different configurations shows that the accuracy of particle positioning, as well as the deviation from the center of the target area, improves significantly when the system uses two microbubbles instead of one. Primarily, during the two-microbubble procedure, there were no instances in which the particles could evade the vortices without undergoing substantial manipulation. In contrast, previous research has shown that particles situated outside the effective streaming range and far from the vortex's core encounter difficulties in achieving full alignment with the desired target. In some cases, they may never attain the intended position.

4 Conclusions

In this study, we introduce an automated microfluidic bead sorter that can accurately position single particles with a precision of tens of micrometers. Notably, this system does not require additional structures to precondition the flow for particle sorting, such as the pre-focusing of particles using sheath flows. Our technique offers several significant advancements over previous systems that utilize only one microbubble, including the use of advanced algorithms that can operate with two microbubbles, a wider microstreaming effective range, and the ability to operate at faster flow rates and in wider channels. Moreover, our method achieves higher positioning accuracy and allows for faster control over bubble size compared to passive techniques. By utilizing controllable microstreaming as a sorting operator, precise positioning of small particles across the width of a microchannel can be achieved. The controllability of the microstreaming is achieved by modulating the frequency and amplitude of the applied driving force, which enables adaptability to different configurations of the microchannel, including small changes in flow rates and channel geometry. The process of sorting is not reliant on particular attributes of particles such as their size, shape, density, or compressibility. This methodology is broadly applicable in all microfluidic domains, provided that the particle density is insignificantly distinct from that of the primary fluid. As the concept is not based on moving parts, just an oscillating bubble, the sorting device is robust and does not require any special maintenance or cleaning operations. Due to the optical analysis of the particle position this technology is limited to transparent fluids. Furthermore, the concept requires low numbers of particles to guarantee reliable sorting.

Supplementary Information The online version contains supplementary material available at https://doi.org/10.1007/s10404-023-02645-4.

Funding Open Access funding enabled and organized by Projekt DEAL.

Declarations

Conflict of interest There are no conflicts to declare.

References

Ahmed D, Mao X, Juluri BK, Huang TJ (2009) A fast microfluidic mixer based on acoustically driven sidewall-trapped microbubbles. Microfluidics Nanofluidics 7(5):727

Ahmed D, Ozcelik A, Bojanala N, Nama N, Upadhyay A, Chen Y, Hanna-Rose W, Huang TJ (2016) Rotational manipulation of single cells and organisms using acoustic waves. Nature communicat 7(1):1–11

Armstrong AJ, Marengo MS, Oltean S, Kemeny G, Bitting RL, Turnbull JD, Herold CI, Marcom PK, George DJ, Garcia-Blanco MA (2011) Circulating tumor cells from patients with advanced prostate and breast cancer display both epithelial and mesenchymal markers. Molecular Cancer Res 9(8):997–1007

Bakhtiari A, Kähler CJ (2022) Automated monitoring and positioning of single microparticle via ultrasound-driven microbubble streaming. Microfluidics Nanofluidics 26(8):1–11

Bischoff FZ, Marquez-Do D, Martinez D, Dang D, Horne C, Lewis D, Simpson J (2003) Intact fetal cell isolation from maternal blood: improved isolation using a simple whole blood progenitor cell enrichment approach (rosettesep^{T}M). Clinical Gentics 63(6):483–489

Chen J, Zheng Y, Tan Q, Zhang YL, Li J, Geddie WR, Jewett MA, Sun Y (2011) A microfluidic device for simultaneous electrical and mechanical measurements on single cells. Biomicrofluidics 5(1):014113

Chen Y, Li P, Huang P-H, Xie Y, Mai JD, Wang L, Nguyen N-T, Huang TJ (2014) Rare cell isolation and analysis in microfluidics. Lab Chip 14(4):626–645

Chen Y, Chung AJ, Wu T-H, Teitell MA, Di Carlo D, Chiou P-Y (2014) Pulsed laser activated cell sorting with three dimensional sheathless inertial focusing. Small 10(9):1746–1751

Cho S, Thielecke H (2007) Micro hole-based cell chip with impedance spectroscopy. Biosensors Bioelect 22(8):1764–1768

Han A, Frazier AB (2006) Ion channel characterization using single cell impedance spectroscopy. Lab Chip 6(11):1412–1414

Khine M, Lau A, Ionescu-Zanetti C, Seo J, Lee LP (2005) A single cell electroporation chip. Lab Chip 5(1):38–43

Malleo D, Nevill JT, Lee LP, Morgan H (2010) Continuous differential impedance spectroscopy of single cells. Microfluidics Nanofluidics 9(2–3):191–198

Marin A, Rossi M, Rallabandi B, Wang C, Hilgenfeldt S, Kähler CJ (2015) Three-dimensional phenomena in microbubble acoustic streaming. Phys Rev Appl 3(4):041001

Marmottant P, Hilgenfeldt S (2003) Controlled vesicle deformation and lysis by single oscillating bubbles. Nature 423(6936):153–156

Mernier G, Piacentini N, Braschler T, Demierre N, Renaud P (2010) Continuous-flow electrical lysis device with integrated control by dielectrophoretic cell sorting. Lab on a Chip 10(16):2077–2082

Nan L, Jiang Z, Wei X (2014) Emerging microfluidic devices for cell lysis: a review. Lab on a Chip 14(6):1060–1073

Nilsson J, Evander M, Hammarström B, Laurell T (2009) Review of cell and particle trapping in microfluidic systems. Analytica chimica acta 649(2):141–157

Rallabandi B, Wang C, Hilgenfeldt S (2014) Two-dimensional streaming flows driven by sessile semicylindrical microbubbles. J fluid mechanics 739:57

Riley N (2001) Steady streaming. Annual Rev Fluid Mechanics 33(1):43–65

Sheng W, Ogunwobi OO, Chen T, Zhang J, George TJ, Liu C, Fan ZH (2014) Capture, release and culture of circulating tumor cells from pancreatic cancer patients using an enhanced mixing chip. Lab on a Chip 14(1):89–98

Shields CW IV, Reyes CD, López GP (2015) Microfluidic cell sorting: a review of the advances in the separation of cells from debulking to rare cell isolation. Lab Chip 15(5):1230–1249

Thameem R, Rallabandi B, Hilgenfeldt S (2016) Particle migration and sorting in microbubble streaming flows. Biomicrofluidics 10(1):014124

Tovar AR, Lee AP (2009) Lateral cavity acoustic transducer. Lab Chip 9(1):41–43

Versluis M, Goertz DE, Palanchon P, Heitman IL, van der Meer SM, Dollet B, de Jong N, Lohse D (2010) Microbubble shape oscillations excited through ultrasonic parametric driving. Phys Rev E 82(2):026321

Volk A (2020) Flow control through ultrasound-driven microbubble streaming. PhD thesis, Universitätsbibliothek der Universität der Bundeswehr München

Volk A, Kähler CJ (2018) Size control of sessile microbubbles for reproducibly driven acoustic streaming. Phys Rev Appl 9(5):054015

Wang C, Jalikop SV, Hilgenfeldt S (2012) Efficient Manipulation Micropart Bubble Streaming Flows. Biomicrofluidics 6(1):012801

Wang C, Rallabandi B, Hilgenfeldt S (2013) Frequency dependence and frequency control of microbubble streaming flows. Phys Fluids 25(2):022002

Wognum AW, Eaves AC, Thomas TE (2003) Identification and isolation of hematopoietic stem cells. Archives Medical Res 34(6):461–475

Yang S, Ündar A, Zahn JD (2006) A microfluidic device for continuous, real time blood plasma separation. Lab on a Chip 6(7):871–880

Zhao M, Schiro PG, Kuo JS, Koehler KM, Sabath DE, Popov V, Feng Q, Chiu DT (2013) An automated high-throughput counting method for screening circulating tumor cells in peripheral blood. Analyt chem 85(4):2465–2471